Materials Today Bio 28 (2024) 101181

Contents lists available at ScienceDirect

Materials Today Bio

journal homepage: www.journals.elsevier.com/materials-today-bio

Waterborne polyurethane nanoparticles incorporating linoleic acid as a potential strategy for controlling antibiotic resistance spread in the mammalian intestine

Gong Li [a,b,c,1], Lu Han [a,b,c,1], Li-Juan Xia [a,c], Ang Gao [a,c], Zhi-Peng Li [a,c], Shi-Ying Zhou [a,c], Lei Wan [a,c], Yao Deng [a,c], Tian-Hong Zhou [a,c], Xin-Yi Lu [a,c], Yang Luo [a,c], Dun-Sheng Liang [a,c], Gui-Ting Wu [a,c], Sheng-Qiu Tang [b], Xin-Lei Lian [a,c], Hao Ren [a,c], Xiao-Ping Liao [a,c], Liang Chen [d,**], Jian Sun [a,c,*]

[a] *Lingnan Guangdong Laboratory of Modern Agriculture, National Risk Assessment Laboratory for Antimicrobial Resistance of Animal Original Bacteria, South China Agricultural University, Guangzhou, PR China*

[b] *Guangdong Provincial Key Laboratory of Utilization and Conservation of Food and Medicinal Resources in Northern Region, Henry Fok School of Biology and Agriculture, Shaoguan University, Shaoguan, 512005, PR China*

[c] *Guangdong Provincial Key Laboratory of Veterinary Pharmaceutics Development and Safety Evaluation, South China Agricultural University, Guangzhou, 510642, PR China*

[d] *Department of Pharmacy Practice, School of Pharmacy and Pharmaceutical Sciences, University at Buffalo, Buffalo, NY, 14214, USA*

ARTICLE INFO

Keywords:
Antimicrobial resistance
Waterborne polyurethane
Conjugation inhibitor
IncX4
Mcr-1

ABSTRACT

Plasmid-mediated conjugative transfer of antibiotic resistance genes (ARGs) within the human and animal intestine represents a substantial global health concern. linoleic acid (LA) has shown promise in inhibiting conjugation *in vitro*, but its *in vivo* effectiveness in the mammalian intestinal tract is constrained by challenges in efficiently reaching the target site. Recent advancements have led to the development of waterborne polyurethane nanoparticles for improved drug delivery. In this study, we synthesized four waterborne polyurethane nanoparticles incorporating LA (WPU@LA) using primary raw materials, including N-methyldiethanolamine, 2,2'-(piperazine-1,4-diyl) diethanol, isophorone diisocyanate, castor oil, and acetic acid. These nanoparticles, identified as $WPU_{0.89}$@LA, $WPU_{0.99}$@LA, $WPU_{1.09}$@LA, and $WPU_{1.19}$@LA, underwent assessment for their pH-responsive release property and biocompatibility. Among these, $WPU_{0.99}$@LA displayed superior pH-responsive release properties and biocompatibility towards Caco-2 and IPEC-J2 cells. In a mouse model, a dosage of 10 mg/kg/day $WPU_{0.99}$@LA effectively reduced the conjugation of IncX4 plasmids carrying the mobile colistin resistance gene (*mcr-1*) by more than 45.1-fold. *In vivo* toxicity assessment demonstrated that 10 mg/kg/day $WPU_{0.99}$@LA maintains desirable biosafety and effectively preserves gut microbiota homeostasis. In conclusion, our study provides crucial proof-of-concept support, demonstrating that $WPU_{0.99}$@LA holds significant potential in controlling the spread of antibiotic resistance within the mammalian intestine.

Abbreviations: AMR, Antimicrobial resistance; HGT, Horizontal gene transfer; GTAs, Phage-like gene transfer agents; ARGs, Antibiotic resistance genes; LA, Linoleic acid; WPU, Waterborne polyurethane; MDEA, N-methyldiethanolamine; CO, Castor oil; MEK, Methyl ethyl ketone; HEP, 2,2'-(piperazine-1,4-diyl) diethanol; IPDI, Isophorone diisocyanate; DBTDL, Dibutyltin dilaurate; AcOH, Acetic acid; ACN, Acetonitrile; LB, Luria-Bertani; EMB, Eosin Methylene Blue; FTIR, Fourier-transform infrared spectroscopy; TEM, Transmission electron microscopy; HPLC, High-performance liquid chromatography; H&E, Hematoxylin and eosin; DLC, Drug loading content; EE, Encapsulation efficiency; DLE, Drug loading efficiency; OTUs, Operational taxonomic units; PCoA, Principal coordinates analysis; WPU@LA, Waterborne polyurethane nanoparticles incorporating LA; ^{1}H NMR, H proton magnetic resonance; GPC, Gel permeation chromatography; THF, Tetrahydrofuran; PBS, Phosphate-buffered saline; SGF, Simulated gastric fluid; SIF, Simulated intestinal fluid.

* Corresponding author. Guangdong Provincial Key Laboratory of Veterinary Pharmaceutics Development and Safety Evaluation, South China Agricultural University, Guangzhou, 510642, PR China

** Corresponding author.

E-mail addresses: liangch@buffalo.edu (L. Chen), jiansun@scau.edu.cn (J. Sun).

[1] Gong Li and Lu Han are co-first authors of the article.

https://doi.org/10.1016/j.mtbio.2024.101181
Received 20 February 2024; Received in revised form 10 July 2024; Accepted 3 August 2024
Available online 10 August 2024

1. Introduction

Antimicrobial resistance (AMR) poses a significant challenge by limiting the effectiveness of antimicrobial agents, impacting both human and animal health [1,2]. This issue is exacerbated by horizontal gene transfer (HGT) among diverse microorganisms [3–5]. Bacteria employ various pathways for HGT, including phage-mediated transduction, transformation through 'naked' DNA, plasmid-mediated conjugation, and mechanisms involving vesicles, nanotubes, and phage-like gene transfer agents (GTAs) [6]. Among these pathways, conjugation is recognized as the most prevalent mechanism [7–9]. For example, naturally occurring plasmids like IncI2, IncX4, and IncX3 increasingly carry antibiotic resistance genes (ARGs) such as *mcr-1* for colistin, $bla_{\text{NDM-1}}$ for carbapenem, and *tet(*X4) for tigecycline [10–12], impacting the treatment of Gram-negative bacterial infections. These plasmids, carrying ARGs, transfer through conjugation between different bacteria, leading to the global dissemination and spread of ARGs. The mammalian gut, known for its diverse microbial population, acts as a reservoir for genetic exchange, strongly linked to the widespread occurrence of conjugation events involving ARGs [13]. Consequently, preventing ARG conjugation, particularly in the mammalian gut, is crucial to mitigate the spread of AMR.

Conjugation involves the transfer of DNA through donor cell-formed conjugative pili to recipient cells [8]. Conjugation of ARGs hinders antibiotic effectiveness, emphasizing its significance in controlling AMR. To tackle this issue, various natural products and small molecules have been developed as conjugation inhibitors. Examples include free nitrous acid, azidothymidine, capsaicin, gingerol analogues, Fe_2O_3@-MoS_2, and abacavir [14–19], but many of these have either shown toxicity or lack *in vivo* testing. Additionally, both Ripoll-Rozada et al. and our previous study have demonstrated that linoleic acid (LA) inhibits the conjugative transfer of IncW, IncH, IncF, IncI, IncL/M and IncX plasmids by suppressing the TrwD ATPase (VirB11 homologue) [20,21].

LA, which is essential for human or animal bodies, is absorbed in the small intestine under acidic pH conditions (pH ~ 2) [22]. However, the challenge arises when considering the normal colon and cecum, which maintain a slightly neutral pH (6.0–7.2) [23]. These regions serve as primary colonization sites for bacteria in the intestinal tract and are key locations for plasmid conjugative transfer. Unfortunately, LA is unable to reach the colon and cecum before its absorption in the small intestine, thereby hindering its potential to inhibit plasmid conjugation in these critical areas. Consequently, the limited pharmacokinetic properties of LA constrain its broader *in vivo* application in conjugation inhibition.

To enhance LA production in the colon and cecum, Peng et al. devised a strategy by constructing a bioactive *Lactobacillus casei* strain LC $^{+\ \text{mcra}}$ by inserting the *mcra* (myosin cross-reactive antigen) gene into the bacterial genome, which promotes the conversion of conjugated LA [24]. On the other hand, when considering drug administration methods, intestinal-based drug delivery is regarded as the preferred approach [25]. Within this context, waterborne polyurethane (WPU), a synthetic high molecular weight polymer, emerges as a versatile material class with applications ranging from coatings to healthcare [26,27]. Recent studies have shown that the integration of N-methyldiethanolamine (MDEA), featuring tertiary amines, plays a pivotal role in the development of pH-responsive polyurethanes [28]. The tertiary amines present in the MDEA segment are widely recognized for their ability to undergo protonation, leading to the formation of an ionic state [29,30]. Consequently, when exposed to acetic acid, the polyurethane with the MDEA segment undergoes ionization, resulting in the formation of zwitterionic polyurethanes. Moreover, a satisfactory nanocarrier usually requires low toxicity [31]. Notably, these zwitterionic polyurethanes have gained significant attention due to their remarkable biocompatibility [32].

This study introduces a novel nanoparticle-based system known as $WPU_{0.99}$@LA, demonstrating its versatility and responsiveness in releasing LA. The effectiveness and safety of this nanocarrier have been robustly established and validated through *in vivo* models. These findings strongly emphasize the promising potential of $WPU_{0.99}$@LA for future applications in inhibiting the spread of AMR within the mammalian intestine.

2. Methods

2.1. Chemicals and bacteria

Castor oil (CO) was purchased from Guangzhou Xinye Co., Ltd. (Guangzhou, China). Linoleic acid (LA), N-methyldiethanolamine (MDEA), and methyl ethyl ketone (MEK) were obtained from Shanghai Rhawn Co., Ltd. (Shanghai, China). 2,2'-(piperazine-1,4-diyl) diethanol (HEP) was obtained from Shanghai Aladdin Reagent Co., Ltd. (Shanghai, China). Isophorone diisocyanate (IPDI) was supplied by Guangzhou Wengjiang Chemical Reagent Co., Ltd. (Guangzhou, China). Dibutyltin dilaurate (DBTDL) was purchased from Fuchen Reagent (Tianjin, China). Acetic acid (AcOH) and phosphoric acid (H_3PO_4) were acquired from Guangzhou Chemical Reagent Factory (Guangzhou, China). Acetonitrile (ACN) was sourced from Shanghai Macklin Biochemical Technology Co., Ltd (Shanghai, China). Human intestinal epithelial cells (Caco-2) and the intestinal porcine enterocyte cell line (IPEC-J2) were procured from Dojindo Chemical Technology (Shanghai, China). Dulbecco's modified Eagle's medium (DMEM, Gibco) and fetal bovine serum (FBS, Gibco) were obtained from Nobimpex Biotechnology (Shanghai, China). Mueller Hinton (MH) broth, Luria-Bertani (LB) broth, LB agar, and Eosin Methylene Blue (EMB) agar were purchased from Guangzhou Huankai Microbial Technology (Guangzhou, China). Streptomycin sulfate and polymyxin sulfate were procured from Beijing Pubo Biotechnology Co., Ltd. (Beijing, China). Antibiotics used for screening and selection procedures were added at the following concentrations (μg/mL): streptomycin sulfate (STR, 2000) and polymyxin sulfate (CS, 2).

Donor strains employed in this study were *E. coli* MQCSZ4GFP, which harbors the conjugative IncX4 plasmid pCSZ4-sfGFP with colistin resistance (*mcr-1*), and a non-conjugative plasmid pMQ expressing mCherry fluorescence protein and LacIq [33]. pCSZ4-sfGFP is a derivative of the clinical IncX4 *mcr-1*-harboring plasmid pCSZ4 [34], and was tagged with the green fluorescent protein (sfGFP) downstream a lacI repressor. *E. coli* C600-lux (streptomycin resistance) was genetically modified by chromosomally tagging with gene cluster *lux*CDABE encoding constitutive bioluminescence. Consequently, donor cells exhibited red fluorescence but GFP expression was inhibited due to the presence of LacIq. Upon the transfer of the pCSZ4-sfGFP plasmid into *E. coli* C600-lux (referred to as the transconjugant), GFP expression became possible without the *lacI* suppression.

2.2. Characterization

Fourier-transform infrared spectroscopy (FTIR) was conducted using a Thermo Fisher Nicolet IS10 FTIR spectrophotometer (Thermo Fisher, Waltham, MA, USA). The H proton magnetic resonance (^{1}H NMR) spectra were recorded on a Bruker AV 600M spectrometer (Karlsruhe, Germany). Gel permeation chromatography (GPC) tests were performed in tetrahydrofuran (THF) solutions at 35 °C with an elution rate of 1.0 mL/min using a Waters 1525 system equipped with a Waters 2414 detector (Burlington, MA, USA). The system was calibrated using polystyrene standards ranging from 200 to 500,000 g/mol. Zeta potential and particle sizes were determined using a Zeta-sizer Nano ZSE instrument (Malvern, Worcestershire, UK). Transmission electron microscopy (TEM) measurements were carried out with an FEI/Talos L120C transmission electron microscope (Thermo Fisher, Pittsburgh, PA, USA) operating at an acceleration voltage of 100 kV. High-performance liquid chromatography (HPLC) measurements were performed with a Waters 2695 instrument (Waters, Milford, MA, USA). Colony images were

captured using the IVIS Lumina LT Series III system (PerkinElmer, Waltham, MA, USA). Histological sections were stained with hematoxylin and eosin (H&E) and observed using a Nikon TE2000U optical microscope (Tokyo, Japan) [35].

2.3. Preparation of WPU and WPU@LA

The representative synthetic route of WPU and WPU@LA is depicted in Fig. 1A. Specifically, a dried double-necked flask was used to introduce CO (3.25 g), IPDI (3.32 g), and HEP (0.4 g), which were then stirred at 78 °C (130–170 r/min) for 10 min to achieve a homogeneous dispersion. The OH group ratio of CO: MDEA: HEP: IPDI was maintained at 1:0.89 (0.99/1.09/1.19):2.15 (2.25/2.35/2.45). Subsequently, 20 μL of DBTDL was added as a catalyst. After 10 min, an appropriate amount of MDEA was added to the solution. MEK (30 mL) was then added to the system and allowed to react for 2 h, followed by cooling the solution to room temperature. Next, AcOH was introduced into the polyurethane chain to counterbalance the presence of free COOH, while being stirred for 30 min.

To synthesize various WPU@LA, 2.35 g of LA was incorporated into the solution. Subsequently, the stirring rate was increased to 300 r/min, and the prepolymer was dispersed in 90 mL of deionized water for 2 h. The successful preparation of both WPU and WPU@LA was achieved through the elimination of MEK in the emulsion via vacuum distillation. Furthermore, 5 mg of WPU@LA was dissolved in 2 mL of methanol, sonicated until fully dissolved, and then filtered through a 0.22 μm microporous membrane. The drug loading content (DLC), encapsulation efficiency (EE), and drug loading efficiency (DLE) of LA were quantitatively determined using HPLC with an Agilent Eclipse XDB-C18 column (4.6 mm × 250 mm, 5 μm) and a mobile phase consisting of acetonitrile and 0.05 % H_3PO_4 (v/v = 10:90) at a flow rate of 1.0 mL/min, maintained at 30 °C, and monitored at 203 nm [36]. DLC (%) and DLE (%) were calculated as described in a previous article [37]. Encapsulation efficiency was calculated as follows: Encapsulation efficiency (%) = (Actual drug loaded)/(Theoretical drug loaded) * 100 [38].

2.4. The LA release rate in vitro

The release amount of LA from WPU@LA *in vitro* was tested according to a dialysis method [37]. Briefly, the release medium contained a phosphate-buffered saline (PBS) solution, 30 % ethanol, and 0.5 % sodium dodecyl sulfate, adjusted to pH = 2.0, 5.8, or 7.4 with hydrochloric acid. 0.5 g of WPU@LA was transferred into dialysis bags (MWCO 3.5 kDa) and suspended in 100 mL of release medium at 37 °C, stirred at 120 rpm. At 0, 0.5, 1, 2, 4, 6, 8, 10, 12, 24, 48, and 96 h post dialysis, 2 mL aliquots were taken for the determination of released LA, measured using a Waters 2695 instrument, and monitored at 203 nm.

2.5. In vitro biocompatibility assay

Caco-2 and IPEC-J2 cells were seeded in 24-well culture plates (1.0×10^5 cells per well) and allowed to adhere for 18 h. Samples of different WPU@LAs were added to each well at final concentrations of 400, 200, 100, 50, 25, 12.5, and 0 μg/mL and incubated for 12 h 10 μL of cell counting Kit-8 (CCK-8) was added to the medium and incubated at 37 °C, 5 % carbon dioxide in the dark for 2 h, and the solution absorbance was measured at 450 nm. Cell viability (%) was calculated using the equation: $(A_{sample}/A_{control}) \times 100$ %, where A_{sample} represents the absorbance of cells treated with the samples, and $A_{control}$ represents the absorbance of the untreated cells [38]. Cell viability was also assessed using a live and dead cell staining kit for Caco-2 and IPEC-J2 cells. These cells were incubated at 37 °C for 24 h, washed with sterile PBS, and then 250 μL of detection buffer containing 0.1 % Calcein-AM/PI was added. The plate was incubated at 37 °C for 30 min, and cell images were observed using a fluorescence microscope [39,40].

2.6. Stability

The stability of $WPU_{0.99}$@LA nanoparticles was evaluated under simulated gastric and intestinal conditions (Hu et al., 2016). Simulated gastric fluid (SGF) and simulated intestinal fluid (SIF) solutions were prepared according to the Chinese Pharmacopoeia (2015) [37]. Briefly, 1 mL of freshly prepared nanoparticles was added to 9 mL of SGF (pH 2) or SIF (pH 6.8), followed by incubation at 37 °C for 6 h [41]. Particle size and zeta potential were measured after each incubation.

2.7. Animal

C57BL/6J mice (SPF, 6 weeks, female) were housed at the Laboratory Animal Center of Southern Medical University, Guangzhou, China. Animal care was conducted in accordance with the guidelines of the American Association for Accreditation of Laboratory Animal Care criteria (2022c045). The mice were allowed to acclimate for 7 days prior to experimentation. All animal experiments were carried out in compliance with the institution's guidelines for animal use and the Guide for the Care and Use of Laboratory Animals at the Laboratory Animal Center of South China Agricultural University (Guangzhou, China).

2.8. In vivo conjugation experiments

All mice were divided into four groups, each consisting of eight mice. Prior to the experiment, all mice were administered STR through oral gavage (200 μL, 5 mg/mL) and drinking water (5 mg/mL) for three days to eliminate colonization resistance. Following this pretreatment, all mice were intragastrically administered a mixture of donor *E. coli* MQCSZ4GFP and recipient *E. coli* C600-lux, with a concentration of approximately 10^8 CFU. Subsequently, the mice were further treated via daily gavage of 10 mg/kg $WPU_{0.99}$@LA, 8 mg/kg $WPU_{0.99}$@LA, or 2 mg/kg LA into the intestinal tract, with the control group receiving an equal volume of sterile water. Fecal samples were obtained on days 1, 2, 3, 5, and 7, and subsequently homogenized by vortexing. The bacterial populations were evaluated through selective plating on EMB agar, enabling the identification of recipient bacteria (STR2000) and transconjugants (STR2000+CS2). The presence of *mcr-1* in the transconjugants was confirmed by PCR and sequencing. The reaction mixture (25 μL) contained 12.5 μL Green Taq MIX (Novizan, Nanjing, China), 2 μL of each primer, 1 μL DNA template, and 9.5 μL nuclease-free water. The PCR procedure was performed using the following reaction conditions: initial denaturation at 98 °C for 3 min followed by 30 cycles of 95 °C for 10 s, 56 °C for 30 s and 72 °C for 30 s, with a final extension at 72 °C for 5 min. The primers for *mcr-1* were GCGTGATGCCAGTTTGCTTA (mcr-F) and GCACATCGACGGCGTATTC (mcr-R). The conjugation frequency was determined by dividing the number of detected transconjugants by the total count of recipients. The conjugation rate was determined by the number of mice with transconjugants in the feces per the total number of mice in each group.

2.9. In vivo biocompatibility assay

For acute toxicity, mice were intravenously injected with 0.2 mL of $WPU_{0.99}$@LA at doses of 5000 mg/kg according to the Guidelines of Animal Drug Acute Toxicity Study (the Center for Veterinary Drug Evaluation of Ministry of Agriculture, 2012) [42]. The time of death was recorded daily for 2 weeks [43]. Then, uninfected mice were randomly assigned to two groups (n = 5/group) for a 2-week treatment period via oral gavage: $WPU_{0.99}$@LA (10 mg/kg/day) and a control group receiving sterile water. The mice were weighed and monitored daily throughout the study. After 2 weeks of $WPU_{0.99}$@LA or sterile water administration, the mice were euthanized. Liver, spleen, duodenum, kidney, stomach, and colon tissues were collected and fixed overnight in 4 % (v/v) PBS-buffered paraformaldehyde. Subsequently, the tissues

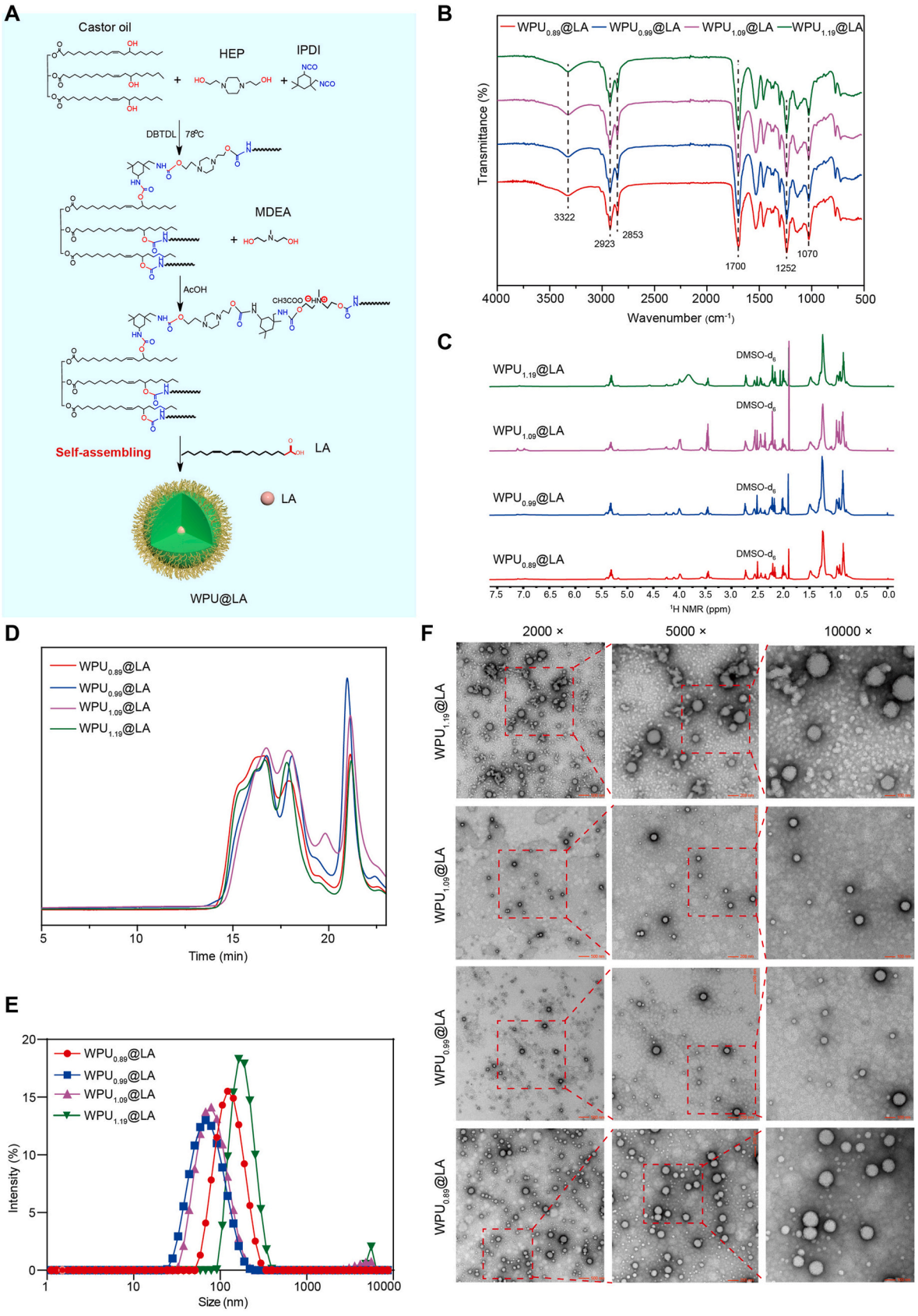

Fig. 1. Synthesis and characterization of WPU, WPU@LA nanomaterials. **(A)** Schematic of the synthesis of WPU@LA nanomaterials. **(B)** FTIR spectrum, **(C)** ^{1}H NMR, **(D)** GPC, **(E)** particle size distribution and **(F)** TEM images, respectively, of four WPU@LAs. HEP, 2,2'-(piperazine-1,4-diyl) diethanol. IPDI, isophorone diisocyanate. DBTDL, dibutyltin dilaurate. MDEA, N methyldiethanolamine. AcOH, acetic acid. LA, linoleic acid, scale bar: 500 nm, 200, and 100 nm, respectively.

were embedded in paraffin, cut into 5 μm sections, stained with H&E, and observed using Nikon TE2000U optical microscopy (Tokyo, Japan) [35,44]. 16S rRNA sequencing was performed following the procedures outlined in a previous study [45].

2.10. Statistical analysis

Statistical analyses and data visualization were conducted using a two-tailed Student's t-test, Kruskal-Wallis test, or Tukey's test with one-way ANOVA (Prism 8.0, GraphPad Software Inc., San Diego, CA, USA). Statistical significance was indicated as follows: * for $p < 0.05$.

3. Results and discussion

3.1. Synthesis and characterization of WPU and WPU@LA nanomaterials

To create a pH-responsive WPU system, we employed MDEA, HEP, IPDI, CO, and AcOH for synthesizing hydrophilic and hydrophobic structures to encapsulate LA (Fig. 1A). MDEA acted as an internal emulsifying agent, influencing emulsification [46]. Increasing MDEA proportions shifted the solution appearance from translucent to milky white, indicating enhanced emulsification efficiency (Table 1). Within WPU carriers, nucleophilic addition reactions occurred between hydroxyl groups in CO, HEP, and MDEA with isocyanate groups in IPDI, forming polyurethane with urethane bonds. Specifically, CO's long fatty acid chain served as the soft segment, providing material flexibility, while HEP and MDEA acted as hard segments, with HEP being pH-responsive [47]. The NCO groups on IPDI acted as crosslinkers, forming polymer chains [48]. By optimizing material proportions, aqueous polyurethane WPU@LA with varying MDEA concentrations (0.89, 0.99, 1.09, and 1.19) were synthesized with respective yields of 87.8 % (w/w), 92.1 % (w/w), 75.2 % (w/w), and 86.4 % (w/w), respectively (Table 1). Fourier-transform infrared (FTIR) spectrum exhibited typical features of WPU at 3321 cm^{-1} (-N-H-), 1252 cm^{-1} (-C-N-), 1700 cm^{-1} (-C=O), and 1070 cm^{-1} (-C-O-C-) (Fig. 1B), confirming reaction between reactant hydroxyl and isocyanate groups to form polyurethane with urethane functional groups containing amino formate.

As shown in Fig. 1C, H NMR spectra peaks at δ5.32 ppm are attributed to the carbon-carbon double bonds of the fatty acid chains from castor oil. New peaks appear at δ3.99 and δ3.44 ppm, corresponding to the proton signals of the ethanoyloxy and acetoxy groups (OCH_2 and OCH) in the esters formed from the esterification of HEP, MDEA, and CO with IPDI. Molecular weight by GPC analysis showed number-average molecular weights of four WPU@LAs as 8407 (PDI = 1.47), 7102 (PDI = 1.37), 6334 (PDI = 1.27), and 8103 (PDI = 1.38) g/mol, respectively (Fig. 1D and Table S1). The high molecular weights of the obtained WPU@LAs could be beneficial for the formation of supramolecular polymeric materials [37]. WPU@LAs exhibited diameters ranging from 68.1 nm to 164.0 nm (Fig. 1E). TEM images further confirmed the spherical morphology of the WPU@LAs (Fig. 1F). Zeta potential of WPU@LA nanoparticles ranged from 23.0 to 52.0 mV (Table 1), indicating a cationic polymer. Together, these results confirm the successful preparation of WPU@LA nanoparticles.

3.2. WPU@LA nanomaterials exhibit promising pH-responsive LA release capability

To investigate the pH-responsive release of LA from various WPU@LAs, solutions with pH values of 2.0, 5.8, and 7.4 were prepared to simulate conditions in the gastrointestinal tract. As illustrated in Fig. 2, minimal release was observed at lower pH (pH = 2), with increased release correlating with higher hydroxide ion concentrations in the medium. The cohesive assembly and release behavior of cationic WPUs are influenced by their similar structures and electrostatic interactions. Hence, monomers with multiple hydroxyl groups (e.g., CO) and positively charged monomers like HEP and MDEA were deliberately chosen. IPDI was slightly in excess during stepwise copolymerization in a butanone solution, decisions driven by the physical properties of WPU. The pH variations trigger conformational changes in microspheres due to positively charged HEP, thereby modulating the amount of released LA [49]. Notably, increasing MDEA ratio significantly enhanced LA release. This can be attributed to MDEA acting as a chain extender. Higher MDEA content reduces cationic WPU chain length, diminishing cross-linking and accelerating release rates [50]. These findings robustly underscore the promising pH-responsive LA release capabilities of the four cationic WPU@LAs.

3.3. In vitro cytotoxicity of WPU@LA

Before considering *in vivo* application, addressing the biosafety of the system is paramount. To assess their suitability for *in vivo* use, we initially evaluated the cytotoxicity of four WPU@LAs using Caco-2 and IPEC-J2 cell lines, commonly employed for *in vitro* cytotoxicity assessments [51,52]. Cell viability was assessed by exposing Caco-2 and IPEC-J2 cells to WPU@LA concentrations ranging from 12.5 to 400 μg/mL. Viability levels remained above 90 % after treatment with $WPU_{0.89}$@LA, $WPU_{0.99}$@LA, and $WPU_{1.19}$@LA at concentrations from 12.5 to 200 μg/mL. However, viability dropped to 32.98 % with 200 μg/mL of WPU1.09@LA for Caco-2 cells (Fig. 3A). Similarly, for IPEC-J2 cells, viability was above 90 % with 200 μg/mL $WPU_{0.99}$@LA, whereas viability significantly decreased in the other three groups. Notably, the 200 μg/mL $WPU_{1.09}$@LA group exhibited the lowest cell viability, at only 6.99 % (Fig. 3B). Additionally, live/dead cell staining for Caco-2 and IPEC-J2 at 200 μg/mL indicated minimal toxicity for $WPU_{0.99}$@LA (Fig. 3C and Fig. S1). Given its lower cytotoxic effect and superior release properties, $WPU_{0.99}$@LA was selected for subsequent experiment.

3.4. $WPU_{0.99}$@LA improves the inhibition of conjugation of mcr-1-harboring IncX4 plasmid in vivo

As emulsions undergo digestion in gastrointestinal conditions, the stability determines how quickly they digest [53]. To explore their potential as oral delivery vehicles, the stability of $WPU_{0.99}$@LA under simulated gastric (SGF) and intestinal (SIF) conditions was determined, respectively. As shown in Fig. S2, minimal changes in particle size and

Table 1
Fundamental characteristics of $WPU_{0.99}$ and WPU@LA nanoparticles.

Nanoparticle	Functional OH (castor oil)	HEP	MDEA	NCO (IPDI)	Appearance	Z-average size (nm)	Zeta potential (mV)	Solids content	Drug loading efficiency	Encapsulation efficiency
$WPU_{0.89}$@LA	1	0.25	0.89	2.15	Translucent	122.2	23	20.7 %	14.16 %	87.8 %
$WPU_{0.99}$@LA	1	0.25	0.99	2.25	Translucent	68.1	52	22.1 %	16.40 %	92.1 %
$WPU_{1.09}$@LA	1	0.25	1.09	2.35	Oyster white	78.8	27.6	19.3 %	13.16 %	75.2 %
$WPU_{1.19}$@LA	1	0.25	1.19	2.45	Oyster white	164.0	33.1	18.7 %	15.88 %	86.4 %
$WPU_{0.99}$	1	0.25	0.99	2.25	Translucent	15.7	15.1	16.8 %	0 %	–

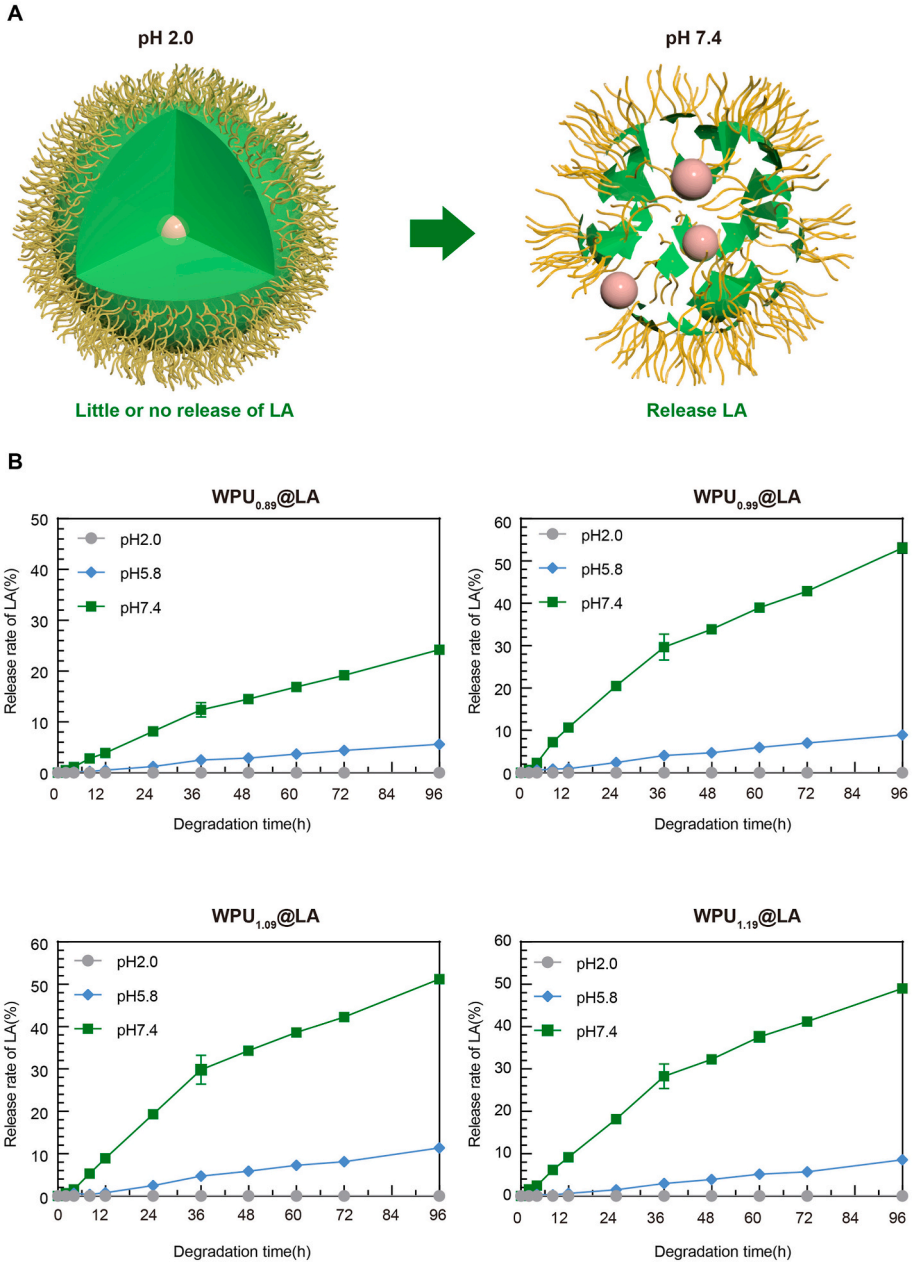

Fig. 2. WPU@LA nanomaterials exhibit promising pH-responsive LA release capability. (A) Schematic of the release of LA from nanoparticle $WPU_{0.89}$@LA, $WPU_{0.99}$@LA, $WPU_{1.09}$@LA and $WPU_{1.19}$@LA under different pH conditions. **(B)** LA release profiles of $WPU_{0.89}$@LA, $WPU_{0.99}$@LA, $WPU_{1.09}$@LA, and $WPU_{1.19}$@LA within 96 h.

zeta potential were observed in SGF, indicating that $WPU_{0.99}$@LA remains stable under gastric condition. However, prolonged incubation in SIF led to a continuous increase in zeta potential and gradual enlargement of particle size, indicating poorer stability of $WPU_{0.99}$@LA under intestinal condition. This underscores our targeted delivery approach to ensure the predominant release of LA in the intestinal environment.

The gut harbors trillions of densely colonizing bacteria that actively combat pathogens, a phenomenon commonly known as "colonization resistance" [54]. Colonization resistance limits the colonization of donor and recipient bacteria in the gut and the subsequent transfer of plasmids [55,56]. To evaluate the efficacy of $WPU_{0.99}$@LA *in vivo* on plasmid conjugation, we initially treated mice with streptomycin to reduce intestinal microbiota, rendering mice susceptible to colonization by exogenous donor and recipient (Fig. 4A). As expected, Fig. 4B shows a significantly reduced colonization level of Enterobacteriaceae (below detection limits) after one day of streptomycin treatment, indicating abnormal changes in intestinal flora amounts and microbiota destruction. Conjugation experiments employed E. coli MQCSZ4GFP as the donor and E. coli C600-lux as the recipient. E. coli MQCSZ4GFP exhibited red fluorescent, while *E. coli* C600-lux expressed bioluminescent luciferase. Transconjugants displayed both green fluorescence and luciferase activity (Fig. 4C), facilitating clear observation of conjugation events. Colony imaging and PCR results confirmed that the IncX4 plasmid pCSZ4-sfGFP could undergo conjugative transfer within the mammalian gut (Fig. 4D–F).

Based on pre-experiment results, both 50 mg/kg $WPU_{0.99}$@LA and 10 mg/kg $WPU_{0.99}$@LA reduced conjugation rates in the *in vivo* experiment (data not shown). To explore potential factors mediating the inhibition of conjugation, we synthesized $PU_{0.99}$ and conducted a subsequent *in vivo* experiment (Table 1). Mice were administered with 10 mg/kg $WPU_{0.99}$@LA, 8 mg/kg $WPU_{0.99}$, 2 mg/kg LA, or sterile water, respectively. Within the first three days post-infection, the conjugation

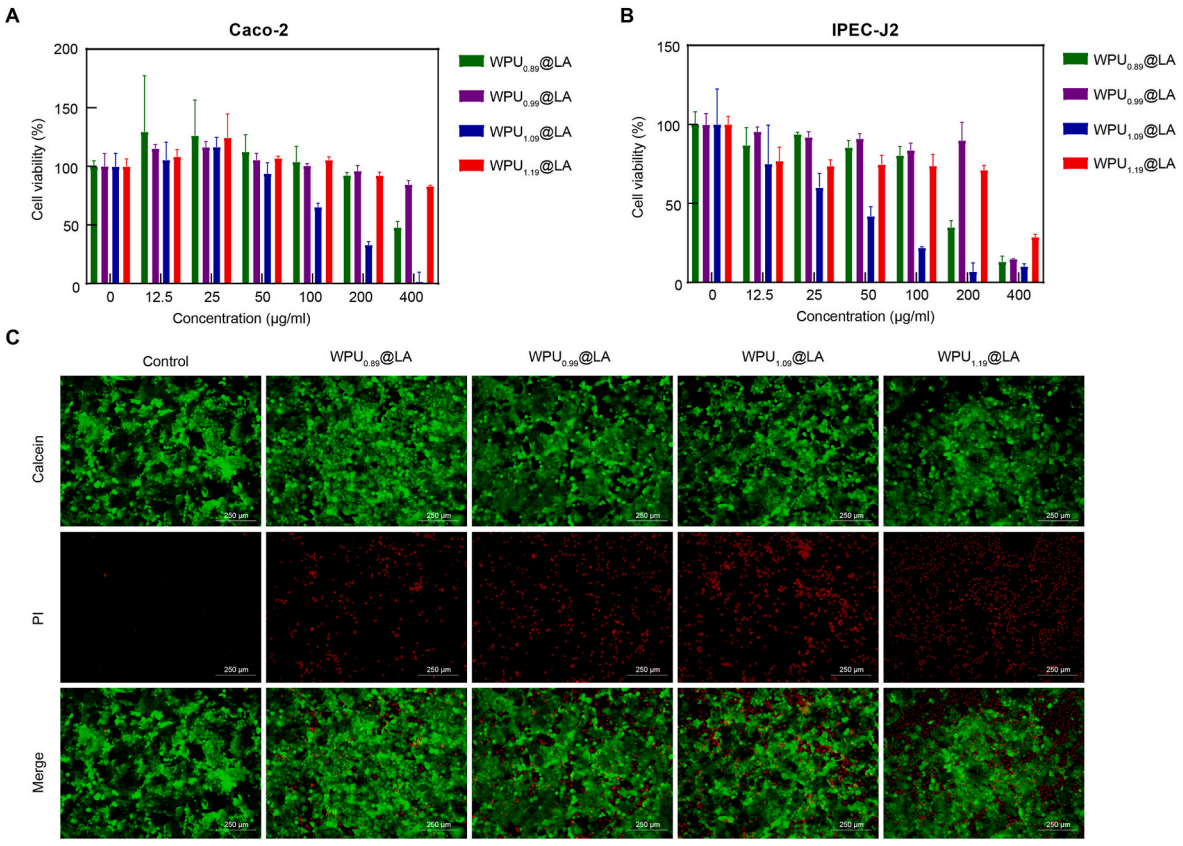

Fig. 3. ***In vitro*** **cytotoxicity of WPU@LAs.** Cell proliferation rate (%) of Caco-2 cells **(A)** and IPEC-J2 cells **(B)** after the treatment with $WPU_{0.89}$@LA, $WPU_{0.99}$@LA, $WPU_{1.09}$@LA and $WPU_{1.19}$@LA nanoparticles for 24 h. **(C)** Live/dead cell staining of Caco-2 cells using 100 μg/ml test samples. scale bar: 250 μm.

rates for the control group were 100 %, 100 %, and 75 %, respectively. In contrast, for the $WPU_{0.99}$@LA group, rates were 100 %, 37.5 %, and 25 %, respectively (Fig. 4G). Conjugation rates in the $WPU_{0.99}$ and LA groups were similar to those in the control group. Similarly, compared to the control group, on day 1, the conjugation frequency in the $WPU_{0.99}$ group decreased by 3.3-fold ($p < 0.05$), and in the $WPU_{0.99}$@LA group, it decreased by 3.0-fold ($p < 0.05$). However, no conjugation inhibition was observed in the samples collected in the $WPU_{0.99}$ group on day 2. Meanwhile, compared to the control group, the conjugation frequency in the $WPU_{0.99}$@LA group decreased by 45.1-fold ($p < 0.05$) (Fig. 4H).

The aforementioned findings highlight the potential of $WPU_{0.99}$@LA in reducing *in vivo* plasmid transfer, indicating its efficacy in mitigating plasmid dissemination within living organisms. Specifically, $WPU_{0.99}$@LA could effectively deliver LA to the site of plasmid conjugation. LA exerts inhibitory effects on VirB11 activity and the expression of its associated genes [20,21]. This inhibition can potentially lower ATP levels, thereby hindering plasmid transfer. Consequently, the inhibitory effect of $WPU_{0.99}$@LA can be attributed to the synergy between LA and the responsive-release $WPU_{0.99}$ carrier.

3.5. *$WPU_{0.99}$@LA demonstrates excellent biocompatibility*

As conjugation inhibitors act preventively without directly triggering therapeutic responses, their practical application requires administration in the mammalian intestine, where plasmid conjugation occurs [57]. Therefore, the conjugation inhibitor must demonstrate favorable biosafety upon entering the human or animal body through the digestive system [57,58]. Initially, an acute toxicity assay was conducted to evaluate the safety of $WPU_{0.99}$@LA *in vivo*. The results indicated that the LD_{50} value for $WPU_{0.99}$@LA in C57BL/6J mice exceeded 5000 mg/kg, with no deaths observed among the 10 mice tested (Fig. S3).

Subsequently, treatment biosafety was evaluated by monitoring changes in body weight and examining organ tissue sections using H&E staining (Fig. 5A). Throughout the experiment, mice receiving 10 mg/kg/day $WPU_{0.99}$@LA did not exhibit significant differences in body weight compared to those receiving sterile water (Fig. 5B). Since organs involved in digestion and metabolism often encounter and accumulate chemicals [59]. We pathologically examined the liver, kidney, spleen, stomach, duodenum, and colon of treated mice using H&E staining. Fig. 5C shows that no damage or inflammation was evident in these organs of mice treated with $WPU_{0.99}$@LA. These findings underscore the excellent biosafety profile of $WPU_{0.99}$@LA, confirming its suitability for *in vivo* use in conjugation inhibition.

3.6. *$WPU_{0.99}$@LA maximally maintains the gut microbiota homeostasis*

The composition of the microbiota in the mammalian gut is intricately linked to both health and disease [60,61]. To assess the impact of $WPU_{0.99}$@LA exposure on the gut microbiota of mice, we conducted 16S rRNA gene sequencing. A total of 294 operational taxonomic units (OTUs) were identified across all samples from the biosafety assay, with 185 unique OTUs in the control group and 151 in the $WPU_{0.99}$@LA group (Fig. 6A). α-diversity was assessed using the Chao1 and Shannon indexes, revealing no significant difference between the two groups [62]. Principal Coordinates Analysis (PCoA) based on Unweighted_Unifac and Bray-Curtis distance indicated a tendency of separation between the two groups (Fig. 6B–F), suggesting differences in the overall structure of gut microbiota [63]. At the phylum level, 8 phyla were detected in all samples, including Bacteroidetes, Firmicutes, Actinobacteria, Verrucomicrobia, Proteobacteria, TM7, Tenericutes, and Deferribacteres (Fig. 6G). Predominantly, Bacteroidetes, Firmicutes, Actinobacteria, and Verrucomicrobia were observed among the gut microbiota from all tested animals. The Firmicutes/Bacteroidetes ratio is an important parameter for evaluating the distribution of gut microbiota

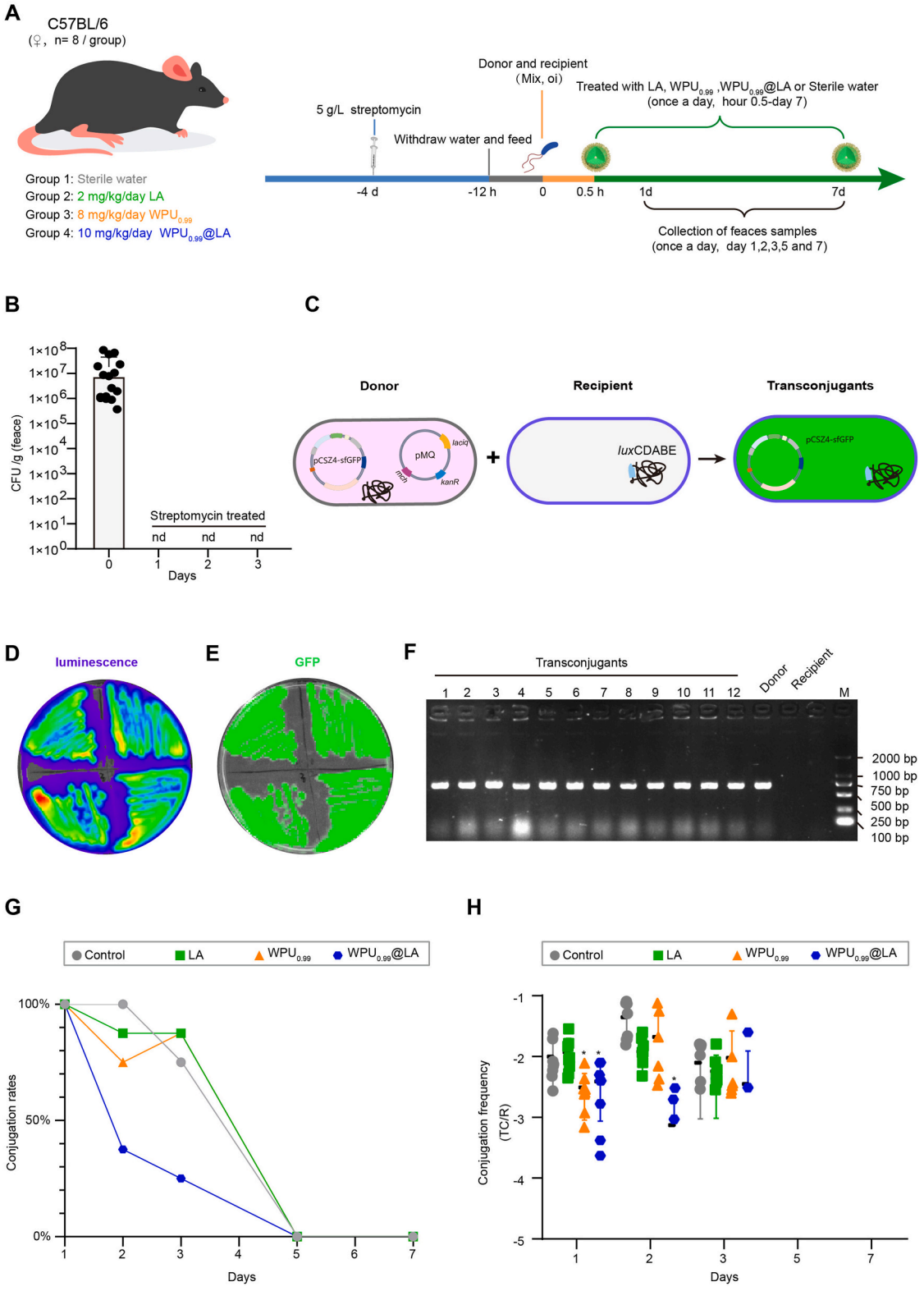

Fig. 4. $WPU_{0.99}$@LA improves the inhibition of conjugation of *mcr-1*-harboring IncX4 plasmid *in vivo*. **(A)** The study protocol including streptomycin pre-treatment, donor and recipient inoculation, and mice with the following treatments: sterile water, 2 mg/kg/day LA, 8 mg/kg/day $WPU_{0.99}$ and 10 mg/kg/day $WPU_{0.99}$@LA. **(B)** Enterobacteriaceae depletion followed by CFU counts from feces of mice treated with 5 g/L streptomycin. **(C)** Development of fluorescence-based strains to monitor transfer of plasmid *in vivo*. Isolated transconjugants were plated on selective media and grown at 37 °C for 24 h. (D) Representative bioluminescence images of transconjugants in the bioluminescence channel. **(E)** Representative green fluorescence (GFP) images of transconjugants in the GFP channel. **(F)** Colony PCR for the *mcr-1* gene using mcr-F and mcr-R as specific primers. Line1-12: PCR product for transconjugants colony; Line13, PCR product for donor (*E. coli* MQCSZ4GFP); Line13, PCR product for recipient (*E. coli* C600-lux). **(G)** Conjugation rates and **(H)** Conjugation frequency in response to sterile water, 2 mg/kg/day LA, 8 mg/kg/day $WPU_{0.99}$ and 10 mg/kg/day $WPU_{0.99}$@LA. Filled icons show individual values for each dataset. Bar graphs represent the average and error bars the standard deviation of the data set. n = 8, *, $p < 0.05$.

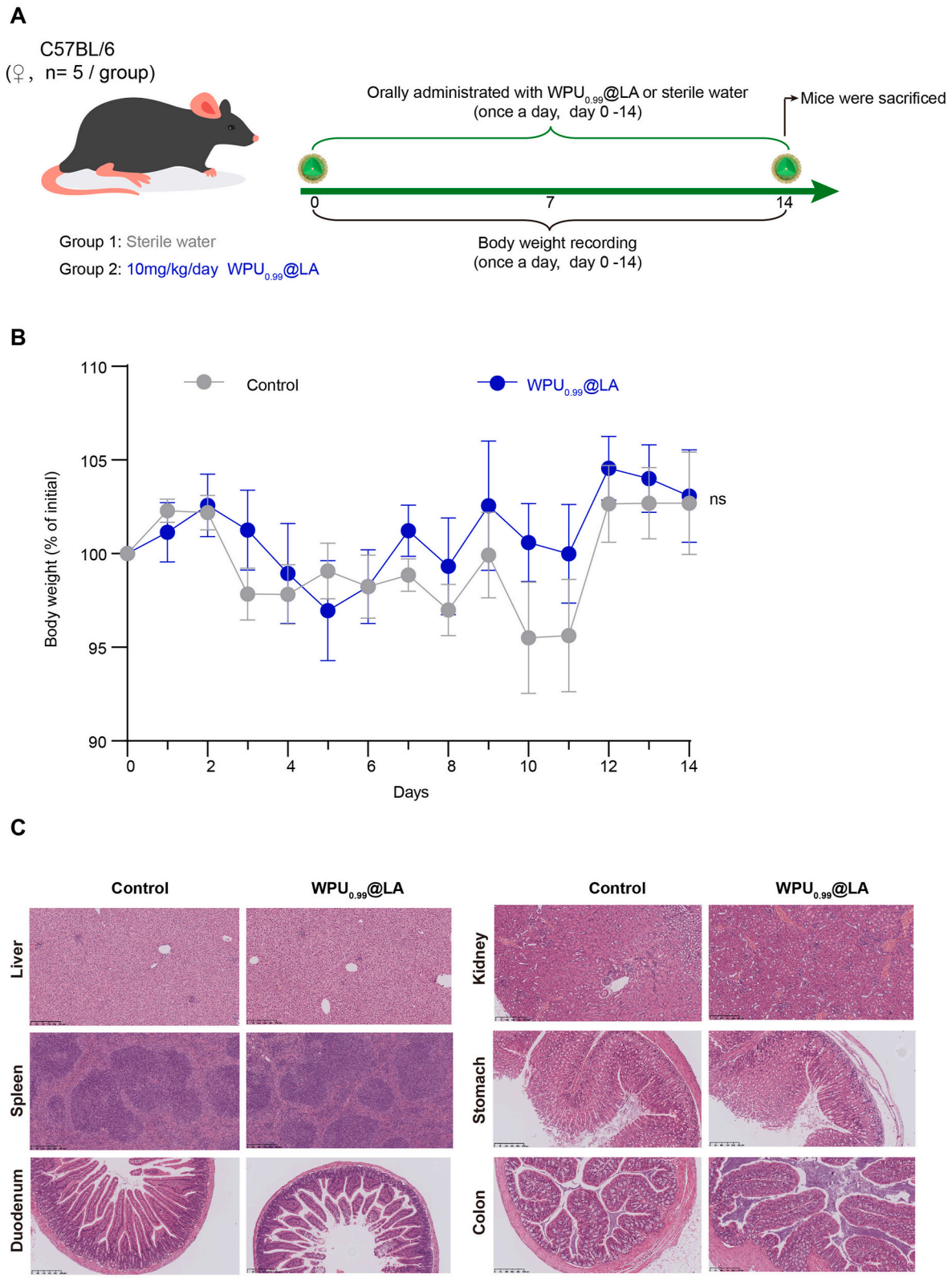

Fig. 5. $WPU_{0.99}$@LA demonstrates excellent biocompatibility. (A) Schematic illustration of the workflow of animal experiments. **(B)** Body weight alteration of mice received the sterile water and $WPU_{0.99}$@LA. **(C)** Pathological examination of liver, kidney, spleen, stomach, duodenum and colon of mice received sterile water and WPU0.99@LA, scale bar: 250 μm. n = 5, *, $p < 0.05$.

[64]. Firmicutes/Bacteroidetes ratio and the relative abundance of Bacteroidota, Firmicutes, Actinobacteria, Verrucomicrobia, and Proteobacteria did not significantly differ between the $WPU_{0.99}$@LA and control group (Fig. 6H–N). These findings suggest that $WPU_{0.99}$@LA maintains gut microbiota homeostasis effectively.

Despite these findings, our study has several limitations. Firstly, our research solely focused on the inhibitory effect of the $WPU_{0.99}$@LA nanoparticle on the IncX4 plasmid. Additionally, we investigated the

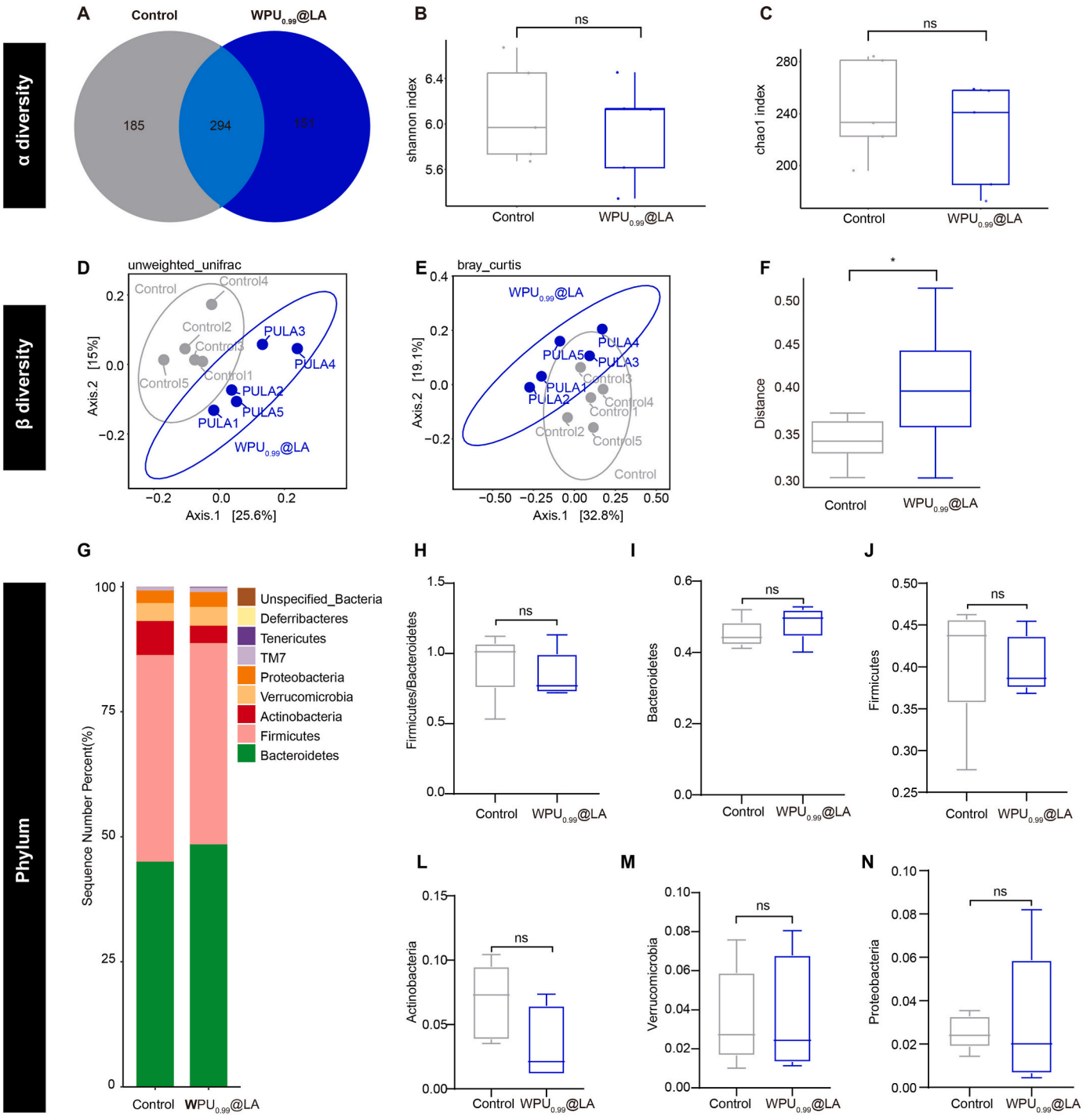

Fig. 6. $WPU_{0.99}$@LA maximally maintains the gut microbiota homeostasis. Operational taxonomic units (OTUs) **(A)**, Shannon index **(B)**, chao1 index **(C)**, Unweighted UniFrac principal coordinate analysis (PCA) **(D)**, Bray Curtis **(E)**, Bray Curtis distances **(F)** of the microbial composition for two groups. **(G)** The relative abundance of cecal bacteria at the phylum level. The Firmicutes/Bacteroidota ratio **(H)**, the relative abundance of cecal Bacteroidota **(I)**, Firmicutes **(J),** Actinobacteria **(L)**, Verrucomicrobia **(M)** and Proteobacteria **(N).** n = 5 mice/group. *, $p < 0.05$.

plasmid conjugation inhibition effect of $WPU_{0.99}$@LA in a mouse model with disrupted gut microbiota. Future studies should broaden the scope of investigation by exploring the inhibitory effects of $WPU_{0.99}$@LA nanoparticles on a diverse range of AMR plasmids *in vivo*. Additionally, examining the conjugation inhibition efficacy of $WPU_{0.99}$@LA in animal models with intact gut microbiota would enhance the translational relevance of our findings. Addressing these aspects will contribute to a more comprehensive understanding of the potential applications of $WPU_{0.99}$@LA in combating antimicrobial resistance. Nevertheless, this study provides robust proof of concept evidence, supporting that $WPU_{0.99}$@LA hold significant potential in controlling the spread of antibiotic resistance within the mammalian intestine.

4. Conclusions

In summary, the $WPU_{0.99}$@LA nanoparticle was engineered as a pH-responsive polyurethane system, showcasing its capability for the precise delivery of LA. This innovative nanoparticle demonstrated

effectiveness in combating the HGT of ARG-bearing plasmids within the mammalian intestine. Overall, $WPU_{0.99}$@LA exhibited a superior safety profile and offers insights for mitigating the spread of AMR *in vivo*.

Ethics approval

Animal experimentation was approved by the by the ethics Committee of the Laboratory Animal Center of South China Agricultural University (Guangzhou, China), approval number 2020B041.

Consent for publication

Not applicable.

CRediT authorship contribution statement

Gong Li: Writing – original draft, Validation, Methodology, Investigation, Funding acquisition, Data curation. **Lu Han:** Writing – original draft, Software, Investigation. **Li-Juan Xia:** Methodology, Investigation. **Ang Gao:** Investigation. **Zhi-Peng Li:** Investigation. **Shi-Ying Zhou:** Methodology, Investigation. **Lei Wan:** Methodology, Investigation. **Yao Deng:** Investigation. **Tian-Hong Zhou:** Investigation. **Xin-Yi Lu:** Investigation. **Yang Luo:** Validation, Investigation. **Dun-Sheng Liang:** Validation, Methodology, Investigation, Formal analysis. **Gui-Ting Wu:** Investigation. **Sheng-Qiu Tang:** Funding acquisition. **Xin-Lei Lian:** Software, Methodology. **Hao Ren:** Writing – review & editing, Supervision. **Xiao-Ping Liao:** Supervision, Project administration. **Liang Chen:** Writing – review & editing, Visualization, Validation. **Jian Sun:** Writing – review & editing, Validation, Supervision, Project administration, Funding acquisition, Conceptualization.

Declaration of competing interest

The authors declare that they have no known competing financial interests or personal relationships that could have appeared to influence the work reported in this paper.

Data availability

Data will be made available on request.

Acknowledgements

This work was supported by National key research and development program of China (2022YFD1800400), the Foundation for Innovative Research Groups of the National Natural Science Foundation of China (32121004), Local Innovative and Research Teams Project of Guangdong Pearl River Talents Program (2019BT02N054), Guangdong provincial key research and development program (2023B0202150001), National key research and development program of China (2022YFD1802100), Laboratory of Lingnan Modern Agriculture Project (NT2021006), Double first-class discipline promotion project (2023B10564003), the 111 Project (D20008), Guangdong Major Project of Basic and Applied Basic Research (2020B0301030007) and the China Postdoctoral Science Foundation (2023M741221).

Appendix A. Supplementary data

Supplementary data to this article can be found online at https://doi.org/10.1016/j.mtbio.2024.101181.

References

[1] L.-R. Jp, F.-M. A, A. L-L, B. P-E, G. C-P, S.-A. O, Prevention of infective endocarditis and bacterial resistance to antibiotics: a brief review, Spec. Care Dent. : official publication of the American Association of Hospital Dentists, the Academy of Dentistry for the Handicapped, and the American Society for Geriatric Dentistry 39 (6) (2019) 603–609.
[2] F. Nd, T. N, M. L, L. Cl, Antibiotic resistance in pacific island countries and territories: a systematic scoping review, Antibiotics (Basel, Switzerland) 8 (1) (2019).
[3] P.-I. A, S. Id, H.-E. G, et al., Horizontally acquired homologs of xenogeneic silencers: modulators of gene expression encoded by plasmids, phages and genomic islands, Genes 11 (2) (2020).
[4] L. Na, C. Ads, Horizontal transfer of antibiotic resistance genes in clinical environments, Can. J. Microbiol. 65 (1) (2019) 34–44.
[5] H. K, M. H, J. J, J. E, S. A, S. D, Role of horizontal gene transfer in the development of multidrug resistance in Haemophilus influenzae, mSphere 5 (1) (2020).
[6] B.J. Arnold, I.T. Huang, W.P. Hanage, Horizontal gene transfer and adaptive evolution in bacteria, Nat. Rev. Microbiol. 20 (4) (2022) 206–218.
[7] J.P.J. Hall, M.A. Brockhurst, E. Harrison, Sampling the mobile gene pool: innovation via horizontal gene transfer in bacteria, Philosophical transactions of the Royal Society of London Series B, Biological sciences 372 (1735) (2017).
[8] I.L. Brito, Examining horizontal gene transfer in microbial communities, Nat. Rev. Microbiol. 19 (7) (2021) 442–453.
[9] M. Hashimoto, H. Hasegawa, S. Maeda, High temperatures promote cell-to-cell plasmid transformation in Escherichia coli, Biochem. Biophys. Res. Commun. 515 (1) (2019) 196–200.
[10] D. Yong, M.A. Toleman, C.G. Giske, et al., Characterization of a new metallo-beta-lactamase gene, *bla*$_{NDM-1}$, and a novel erythromycin esterase gene carried on a unique genetic structure in *Klebsiella pneumoniae* sequence type 14 from India, Antimicrobial agents and chemotherapy 53 (12) (2009) 5046–5054.
[11] Y.Y. Liu, Y. Wang, T.R. Walsh, et al., Emergence of plasmid-mediated colistin resistance mechanism MCR-1 in animals and human beings in China: a microbiological and molecular biological study, Lancet Infect. Dis. 16 (2) (2016) 161–168.
[12] J. Sun, C. Chen, C.Y. Cui, et al., Plasmid-encoded tet(X) genes that confer high-level tigecycline resistance in Escherichia coli, Nature microbiology 4 (9) (2019) 1457–1464.
[13] R.S. McInnes, G.E. McCallum, L.E. Lamberte, W. van Schaik, Horizontal transfer of antibiotic resistance genes in the human gut microbiome, Curr. Opin. Microbiol. 53 (2020) 35–43.
[14] M. Buckner, M. Ciusa, R. Meek, et al., HIV drugs inhibit transfer of plasmids carrying extended-spectrum β-lactamase and carbapenemase genes, mBio 11 (1) (2020).
[15] H. Huang, J. Liao, X. Zheng, Y. Chen, H. Ren, Low-level free nitrous acid efficiently inhibits the conjugative transfer of antibiotic resistance by altering intracellular ions and disabling transfer apparatus, Water Res. 158 (2019) 383–391.
[16] M.M.C. Buckner, M.L. Ciusa, L.J.V. Piddock, Strategies to combat antimicrobial resistance: anti-plasmid and plasmid curing, FEMS Microbiol. Rev. 42 (6) (2018) 781–804.
[17] H. Wang, H. Qi, M. Zhu, et al., MoS(2) decorated nanocomposite: Fe(2)O(3)@MoS(2) inhibits the conjugative transfer of antibiotic resistance genes, Ecotoxicol. Environ. Saf. 186 (2019) 109781.
[18] M.M.C. Buckner, M.L. Ciusa, R.W. Meek, et al., HIV drugs inhibit transfer of plasmids carrying extended-spectrum β-lactamase and carbapenemase genes, mBio 11 (1) (2020), https://doi.org/10.1128/mbio.03355-19.
[19] B.O. Oyedemi, E.M. Kotsia, P.D. Stapleton, S. Gibbons, Capsaicin and gingerol analogues inhibit the growth of efflux-multidrug resistant bacteria and R-plasmids conjugal transfer, J. Ethnopharmacol. 245 (2019) 111871.
[20] G. Li, L. Xia, S. Zhou, et al., Linoleic acid and α-linolenic acid inhibit conjugative transfer of an IncX4 plasmid carrying *mcr-1*, J. Appl. Microbiol. 130 (6) (2021) 1893–1901.
[21] J. Ripoll-Rozada, Y. García-Cazorla, M. Getino, et al., Type IV traffic ATPase TrwD as molecular target to inhibit bacterial conjugation, Mol. Microbiol. 100 (5) (2016) 912–921.
[22] C.W. Ko, J. Qu, D.D. Black, P. Tso, Regulation of intestinal lipid metabolism: current concepts and relevance to disease, Nat. Rev. Gastroenterol. Hepatol. 17 (3) (2020) 169–183.
[23] N.G. Kotla, S. Rana, G. Sivaraman, et al., Bioresponsive drug delivery systems in intestinal inflammation: state-of-the-art and future perspectives, Adv. Drug Deliv. Rev. 146 (2019) 248–266.
[24] M. Peng, Z. Tabashsum, P. Patel, et al., Prevention of enteric bacterial infections and modulation of gut microbiota with conjugated linoleic acids producing Lactobacillus in mice, Gut Microb. 11 (3) (2019) 433–452.
[25] B. Ye, D.R. van Langenberg, Mesalazine preparations for the treatment of ulcerative colitis: are all created equal? World J. Gastrointest. Pharmacol. Therapeut 6 (4) (2015) 137–144.
[26] D.B. Ju, J.C. Lee, S.K. Hwang, C.S. Cho, H.J. Kim, Progress of polysaccharide-contained polyurethanes for biomedical applications, Tissue engineering and regenerative medicine 19 (5) (2022) 891–912.
[27] M.H.S. Mangal, S. Bose, T. Banerjee, Innovations in applications and prospects of non-isocyanate polyurethane bioplastics, Biopolymers (2023) e23568.
[28] Y. Wang, X. Li, G. Wu, et al., Precise control of drug release from dually responsive poly (ether urethane) nanoparticles, RSC advances 3 (33) (2013) 13859–13868.
[29] R. Liu, Y. Chen, H. Fan, Design, characterization, dyeing properties, and application of acid-dyeable polyurethane in the manufacture of microfiber synthetic leather, Fibers Polym. 16 (2015) 1970–1980.
[30] K. Chen, R. Liu, C. Zou, et al., Linear polyurethane ionomers as solid–solid phase change materials for thermal energy storage, Solar energy materials and solar cells 130 (2014) 466–473.

[31] F. Liu, D. He, Y. Yu, L. Cheng, S. Zhang, Quaternary ammonium salt-based cross-linked micelles to combat biofilm, Bioconjugate Chem. 30 (3) (2019) 541–546.
[32] S. Fu, H. Ren, Z. Ge, H. Zhuo, S. Chen, Shape memory polyurethanes based on zwitterionic hard segments, Polymers 9 (10) (2017) 465.
[33] G. Li, T. Long, S. Zhou, et al., CRISPR-AMRtracker: a Novel Toolkit to Monitor the Antimicrobial Resistance Gene Transfer in Fecal Microbiota, 2023.
[34] J. Sun, L.X. Fang, Z. Wu, et al., Genetic analysis of the IncX4 plasmids: implications for a unique pattern in the mcr-1 acquisition, Sci. Rep. 7 (1) (2017) 424.
[35] R. Lu, X. Zhou, K. Peng, et al., High-density dynamic bonds cross-linked hydrogel with tissue adhesion, highly efficient self-healing behavior, and NIR photothermal antibacterial ability as dressing for wound repair, Biomacromolecules 25 (4) (2024) 2486–2496.
[36] Z.Z.A. B, H.W. A, C.Y. A, et al., Qualitative and quantitative analysis of linoleic acid in polygonati rhizoma, Digital Chinese Medicine 3 (3) (2020) 180–187.
[37] L. Han, X.W. Liu, T. Zang, et al., H(2)S responsive PEGylated poly (lipoic acid) with ciprofloxacin for targeted therapy of Salmonella, J. Contr. Release : official journal of the Controlled Release Society 351 (2022) 896–906.
[38] Y. Yu, P. Li, C. Zhu, N. Ning, S. Zhang, G.J. Vancso, Multifunctional and recyclable photothermally responsive cryogels as efficient platforms for wound healing, Adv. Funct. Mater. 29 (35) (2019) 1904402.
[39] L. Han, T. Zang, L. Tan, et al., Self-assembly of H(2)S-responsive nanoprodrugs based on natural rhein and geraniol for targeted therapy against *Salmonella* Typhimurium, J Nanobiotechnology 21 (1) (2023) 483.
[40] D. He, Y. Yu, F. Liu, et al., Quaternary ammonium salt-based cross-linked micelle templated synthesis of highly active silver nanocomposite for synergistic anti-biofilm application, Chem. Eng. J. 382 (2020) 122976.
[41] S. Hu, T. Wang, M.L. Fernandez, Y. Luo, Development of tannic acid cross-linked hollow zein nanoparticles as potential oral delivery vehicles for curcumin, Food Hydrocolloids 61 (2016) 821–831.
[42] Center for Veterinary Drug Evaluation MoA, Compilation of Guidelines of Veterinary Drug Research Technology (2006–2011), China Chemical Industry Press, Beijing, 2012.
[43] P. Jing, Y. Luo, Y. Chen, J. Tan, C. Liao, S. Zhang, Aspirin-loaded cross-linked lipoic acid nanodrug prevents postoperative tumor recurrence by residual cancer cell killing and inflammatory microenvironment improvement, Bioconjug Chem 34 (2) (2023) 366–376.
[44] P. Li, W. She, Y. Luo, et al., One-pot, self-catalyzed synthesis of self-adherent hydrogels for photo-thermal, antimicrobial wound treatment, J. Mater. Chem. B 9 (1) (2021) 159–169.
[45] A.D. Sklirou, M. Ralli, M. Dominguez, I. Papassideri, A.L. Skaltsounis, I. P. Trougakos, Hexapeptide-11 is a novel modulator of the proteostasis network in human diploid fibroblasts, Redox Biol. 5 (2015) 205–215.
[46] H. Daemi, M. Barikani, M. Barmar, Highly stretchable nanoalginate based polyurethane elastomers, Carbohydr. Polym. 95 (2) (2013) 630–636.
[47] J.P.P. de Morais, I.K.C. Pacheco, A. Filho, et al., Polyurethane derived from castor oil monoacylglyceride (Ricinus communis) for bone defects reconstruction: characterization and in vivo testing, J. Mater. Sci. Mater. Med. 32 (4) (2021) 39.
[48] Y. Xia, Z. Zhang, M.R. Kessler, B. Brehm-Stecher, R.C. Larock, Antibacterial soybean-oil-based cationic polyurethane coatings prepared from different amino polyols, ChemSusChem 5 (11) (2012) 2221–2227.
[49] L. Wang, W. Cao, Y. Yi, H.P. Xu, Dual redox responsive coassemblies of diselenide-containing block copolymers and polymer lipids, Langmuir 30 (19) (2014) 5628–5636.
[50] H. Liang, Q. Lu, M. Liu, et al., UV absorption, anticorrosion, and long-term antibacterial performance of vegetable oil based cationic waterborne polyurethanes enabled by amino acids, Chem. Eng. J. 421 (2021) 127774.
[51] M. Wang, S.K. You, H.K. Lee, et al., Development and evaluation of docetaxel-phospholipid complex loaded self-microemulsifying drug delivery system: optimization and in vitro/ex vivo studies, Pharmaceutics 12 (6) (2020).
[52] C. Yu, P. Lu, S. Liu, et al., Efficiency of deoxynivalenol detoxification by microencapsulated sodium metabisulfite assessed via an *in vitro* bioassay based on intestinal porcine epithelial cells, ACS Omega 6 (12) (2021) 8382–8393.
[53] M. Zhang, X. Li, L. Zhou, W. Chen, E. Marchioni, Protein-based high internal phase pickering emulsions: a review of their fabrication, composition and future perspectives in the food industry, Foods 12 (3) (2023).
[54] F. Spragge, E. Bakkeren, M.T. Jahn, et al., Microbiome diversity protects against pathogens by nutrient blocking, Science 382 (6676) (2023) eadj3502.
[55] K. Neil, N. Allard, F. Grenier, V. Burrus, S. Rodrigue, Highly efficient gene transfer in the mouse gut microbiota is enabled by the Incl2 conjugative plasmid TP114, Commun. Biol. 3 (1) (2020) 523.
[56] B. Stecher, R. Denzler, L. Maier, et al., Gut inflammation can boost horizontal gene transfer between pathogenic and commensal Enterobacteriaceae, Proceedings of the National Academy of Sciences of the United States of America 109 (4) (2012) 1269–1274.
[57] M. Getino, R. Fernandez-Lopez, C. Palencia-Gandara, et al., Tanzawaic acids, a chemically novel set of bacterial conjugation inhibitors, PLoS One 11 (1) (2016) e0148098.
[58] S.-T. Yang, Y. Liu, Y.-W. Wang, A. Cao, Biosafety and bioapplication of nanomaterials by designing protein–nanoparticle interactions, Small 9 (9–10) (2013) 1635–1653.
[59] H. Ren, Y. Pan, J. Zhong, et al., An antibiotic-destructase-activated Fenton-like catalyst for synergistic removal of tetracycline residues from aquatic environment, Chem. Eng. J. 459 (2023) 141576.
[60] C. Kunz, S. Kuntz, S. Rudloff, Intestinal flora, Advances in experimental medicine and biology 639 (2009) 67–79.
[61] M. Tramontano, S. Andrejev, M. Pruteanu, et al., Nutritional preferences of human gut bacteria reveal their metabolic idiosyncrasies, Nature microbiology 3 (4) (2018) 514–522.
[62] Z. He, Y. Ma, S. Yang, et al., Gut microbiota-derived ursodeoxycholic acid from neonatal dairy calves improves intestinal homeostasis and colitis to attenuate extended-spectrum β-lactamase-producing enteroaggregative *Escherichia coli* infection, Microbiome 10 (1) (2022) 79.
[63] F. Pan, L. Zhang, M. Li, et al., Predominant gut *Lactobacillus murinus* strain mediates anti-inflammaging effects in calorie-restricted mice, Microbiome 6 (1) (2018) 54.
[64] C. Brandscheid, F. Schuck, S. Reinhardt, et al., Altered gut microbiome composition and tryptic activity of the 5xFAD alzheimer's mouse model, J Alzheimers Dis 56 (2) (2017) 775–788.